Asymmetry in elastic properties and the evolution of large continental strike-slip faults

Xavier Le Pichon, Corné Kreemer, Nicolas Chamot-Rooke

Asymmetry in elastic properties and the evolution of large continental strike-slip faults

Xavier Le Pichon and Corné Kreemer[1]
Collège de France, Europôle de l'Arbois, Aix-en-Provence, France

Nicolas Chamot-Rooke
Laboratoire de Géologie, Ecole Normale Supérieure, Paris, France

Received 23 July 2004; revised 10 December 2004; accepted 4 January 2005; published 19 March 2005.

[1] We use geodetic studies to quantify several cases of significant asymmetry in interseismic and coseismic effects along large continental strike-slip faults using simple two-dimensional edge dislocation models. We first show that asymmetric elastic loading characterizes the present Main Marmara Fault, a portion of the North Anatolian Fault along the northern margin of the Sea of Marmara. The ratio of asymmetry there is about 10. This ratio is even larger, about 30, along the northern Sumatra fault near lake Toba caldera. We then examine two profiles near Point Reyes and Point Arena across the northern San Andreas Fault that have been previously proposed as affected by asymmetry both in interseismic and coseismic effects. We show that an asymmetry ratio of 1.6 in interseismic loading exists near Point Arena, with the southwest side of the fault being more rigid than the northeast one. On the other hand, we do not find significant asymmetry for the Point Reyes profile that was previously described as highly asymmetric. We examine coseismic motion during the 1906 earthquake along the same two profiles. Ratios of 1.2 and 1.7 are found for the Point Arena and Point Reyes profiles, respectively. We discuss the possible causes of asymmetry. Contrasts in seismic velocity in the brittle portion suggest ratios generally not exceeding 2.5 for the dynamic rigidity in the upper brittle section. Larger ratios may involve other complex causes such as differences between static and dynamic rigidities, contrasts in rheology in the deeper creeping sections, and postseismic transients. We conclude that asymmetry should be systematically included within the parameters to be inverted when dealing with the mechanics of large-scale strike-slip faults.

Citation: Le Pichon, X., C. Kreemer, and N. Chamot-Rooke (2005), Asymmetry in elastic properties and the evolution of large continental strike-slip faults, *J. Geophys. Res.*, *110*, B03405, doi:10.1029/2004JB003343.

1. Introduction

[2] Large faults juxtapose materials that generally have different physical properties. This is obvious for reverse faults because of the vertical stratification of the crust. In this paper, however, we only consider strike-slip faults, for which deformation across the fault is symmetric when material properties are uniform across the fault. Thus, in the simplest case, asymmetry of deformation across the fault reflects asymmetry in material properties. This is not true of other types of faults where asymmetry of deformation is inherently present. We define the asymmetry in the following way. If s is the long-term relative displacement rate across the fault, in the absence of elasticity, the fault slip along the fault is s and results from the motion s of one plate with respect to the other one. In the presence of uniform elastic properties, the displacement rate of the fault is s/2. The elastic effect is symmetric. However, if the elastic properties are different, the elastic effect changes discontinuously across the fault and produces an asymmetry that can be quantified by the ratio s_1/s_2. Now s_1 is the (elastic) displacement rate on one side of the fault and s_2 on the other, with $s_2 = s - s_1$.

[3] We do not consider here oceanic transform faults, because, although asymmetry is expected there, geodetic measurements cannot yet be made to demonstrate the extent of asymmetry. Rather, we consider large-scale continental strike-slip faults where one may actually pass from a fault that juxtaposes an oceanic lithosphere to a continental lithosphere at one extremity, to a continent-continent portion in the middle portion, and to a continent-ocean structure at the other extremity. Such extreme cases exist for the San Andreas, Alpine and Philippine faults. Thus large heterogeneity is often expected to be an intrinsic character of this type of faults. Large heterogeneity may exist at the lithosphere scale, as for the San Andreas Fault (SAF)

[1]Now at Nevada Bureau of Mines and Geology, University of Nevada, Reno, USA.

0148-0227/05/2004JB003343$09.00

[*Melbourne and Helmberger*, 2001], but can also often be present at the upper brittle crust scale. In addition, in this upper brittle portion, repeated earthquake ruptures produce fault gauge material that may reach sizable thickness thus introducing additional heterogeneities, especially in view of the fact that the rupture tends to be localized on one side of the zone of fault breccia [see, e.g., *Ben-Zion and Andrews*, 1998]. Several people [e.g., *Andrews and Ben-Zion*, 1997; *Weertman*, 1980] have shown that if the fault is a material discontinuity interface, the rupture tends to occur as a narrow pulse that propagates in a wrinkle-like mode within the low-rigidity material. The slip pulse is associated with dynamic changes of normal stress in such a way that slip can occur with little loss of energy to friction. This is because the symmetry is broken across the faults and slip can change normal traction. As a result, once an elastic contrast is created across the fault, it tends to localize the rupture along it and to stabilize the fault geometry. Thus, as emphasized by *Ben-Zion and Sammis* [2003], bimaterial interfaces may play a significant role in the genesis and evolution of large faults and especially large strike-slip faults and the method we propose here is one way to detect the presence of this bimateriality.

[4] The repeated seismic ruptures that are responsible for the formation of the faults depend on the elastic properties of the upper brittle portion and the viscoelastic properties of the underlying "ductile" layer. When modeling the seismic cycle, it is often implicitly assumed that these properties are identical on both sides of the fault and thus asymmetry is generally ignored. Yet, one would expect asymmetry to be present in many if not most large ruptures of this type of faults that should be considered as bimaterial faults, and one could solve for the presence of this asymmetry when inverting geodetic data. Contrasts in seismic velocity across a fault do not usually exceed 1.35 [*Ben-Zion and Andrews*, 1998]. From V_s equal to $\sqrt{\mu/\rho}$, with μ the rigidity and ρ the density, and considering that the rigidity μ varies approximately as the seismic velocity to the third power [see, e.g., *Andrews and Ben-Zion*, 1997], and velocity varies in the crust approximately as $\rho^{1.2}$ [*Christensen and Mooney*, 1995], we can infer that the expected maximum elastic parameter ratio is thus about 2.5 (or 2.34 to be exact).

[5] At the beginning of last century, *Reid* [1910] observed an asymmetry in the coseismic motion of the 1906 San Francisco earthquake and stated that "this is probably in part due to the fact that the rocks on the western side are more rigid than those on the eastern side." The Point Reyes geodetic profile measured by *Prescott and Yu* [1986] presented a spectacular asymmetry in strain across the northern SAF as the velocity on the southwestern side was quite constant whereas it showed a linear fairly steep gradient to the southeast. This asymmetry has been subsequently the object of intense discussion. *Li and Rice* [1987, p. 11,546] proposed that the "the upper mantle to the SW of the SAF could be too cool to deform readily and hence could move as an effectively rigid zone" and *Lisowski et al.* [1991] pointed out that lateral inhomogeneity in the brittle crust could be its cause. *Lisowski et al.* [1991] computed simple models assuming a ratio of 5 in rigidity. *Freymueller et al.* [1999, p. 7427] concluded that the velocity field along a profile at the latitude of Point Arena, farther north, is "highly asymmetric about the San Andreas Fault, with almost all sites west of the fault moving at nearly the same rate as Point Reyes." *Kenner and Segall* [2003, paragraph 34] recently noted: "postseismic and interseismic deformation in northern California is asymmetric with respect to the trace of the San Andreas fault." They found that 90 years of post-1906 geodetic data in northern California are best explained by models which include discrete vertical shear zones beneath each of the three subparallel faults in the region and that these models also explain the asymmetry in strain observed. However, they do not consider the possibility that at least part of this asymmetry may be due to a bimaterial San Andreas Fault.

[6] *Lisowski et al.* [1991], following *Rybicki and Kasahara* [1977], pointed out further that the effect of a low-rigidity fault zone is to concentrate deformation within it. This last effect has been later used by [*Chen and Freymueller*, 2002] to propose the presence of a near-fault compliant zone along the SAF in the San Francisco Bay area. *Peltzer et al.* [1999] demonstrated with SAR interferometry that the M_w = 7.6 Manyi (Tibet) strike-slip earthquake had asymmetric, along-strike, displacement profiles between the two sides of the rupture; a pattern that could be explained if the elastic moduli of the crust for regions in tension are different from those in compression, because of the presence of cracks in the crust at shallow depth.

[7] The purpose of this paper is to quantify a few cases of interseismic and coseismic deformation where large asymmetry in strain appears to be present, and to discuss the significance of this asymmetry. Asymmetric ratios of 1.2–1.3 are the lower limit of resolution that we can obtain. With a typical slip rate of 20 mm yr^{-1} and with $\sim$10 mm yr^{-1} loading on each side of the fault, a resolution better than 2 mm yr^{-1} in the velocity estimates is required to resolve this type of small asymmetry. This resolution is probably impossible to obtain with existing data given either the noise or other effects (e.g., nonvertical fault). On the other hand, it should be possible to reliably quantify large asymmetry (i.e., a factor larger than 1.5).

2. Testing for Asymmetric Interseismic Strain

[8] As pointed out by *Savage* [1990, 4878], "even high quality measurements across a transform fault are incapable of defining the deformation mechanism at depth." Our aim is not to define this mechanism but rather to quantify the ratios in presumably mostly elastic deformation along the different segments of faults studied. We wish to use the simplest possible model to test for the asymmetry of strain across faults, which is the model proposed by *Savage and Burford* [1973] for the elastic two-dimensional pure strike-slip case. Their analytical formulation is based on a dislocation model with no slip on the fault above depth D and slip by a constant amount below this surface. It can be derived using a screw dislocation [*Weertman and Weertman*, 1964]. The same analytical solution had earlier been used [*Chinnery*, 1961] as the limiting case of a rectangular dislocation growing to infinity. This analytical very simple model has the great advantage to allow a simple quantitative evaluation of the asymmetry as defined above.

[9] Interseismic velocities near a locked fault which creeps below depth D indicate the accumulated strain at a distance x from the fault as a function of the locking depth

D and the total far-field relative displacement rate s. For a vertical strike-slip fault, the fault parallel velocity $v(x)$ at the Earth's surface can be described as resulting from a screw dislocation along the fault below D. The value of the dislocation is equal to s. The solution is linear in the angle $\theta = \tan^{-1}(x/D)$. If it is a bimaterial fault, the solution is still linear in θ on both sides of the fault but the slips (Burgers vectors) are different. We need to differentiate with respect to time and then add a rigid body translation s_1. This results in a discontinuity in the strain rate component xy across the fault plane that accounts for the continuity of stress, the rigidity ratio being inversely proportional to the strain rate ratio. We thus write

$$v(x) = s_1 + 2\frac{s_2}{\pi}\tan^{-1}\left(\frac{x}{D}\right) \qquad ;x \geq 0$$
$$v(x) = s_1 + 2\frac{s_1}{\pi}\tan^{-1}\left(\frac{x}{D}\right) \qquad ;x < 0 \tag{1}$$

where the fault is at $x = 0$ and x is defined positive on the side of the fault where $v(x) \rightarrow s$ when $x \rightarrow \infty$. As defined earlier, s_1 is the total accumulated velocity at the side where $x < 0$, and s_2 is the accumulated velocity on the fault's opposite side. Thus $s_1 + s_2 = s$; for a symmetric case $s_1 = s_2 = s/2$. The ratio s_2/s_1 directly indicates the rigidity contrast R of both sides of the fault's locked portion. Note that in (1) we have assumed for convenience that $v(x)$ vanishes at $x = -\infty$ but the solution is still valid if a rigid translational movement is added. For our best fitting models presented below we use the L1 norm but present misfits in terms of RMS values. Results are summarized in Table 1.

[10] Because of the strong correlation between D and s [e.g., *Prescott et al.*, 2001], the inversion is quite unstable. We generally fix D to the value obtained in the studies from which we take the data. Fixing D should not alter our investigation in rigidity contrast. Moreover, the value of D that best fits the inversion does not necessarily correspond to the true locking depth, because of the possible effects of lower crustal viscoelasticity on the observed surface deformation [*Kenner and Segall*, 2003; *Malservisi et al.*, 2001; *Savage and Lisowski*, 1998].

2.1. North Anatolian Fault in the Sea of Marmara

[11] *Le Pichon et al.* [2003] found the very large ratio of ~10 in the interseismic strain rate on both sides of the North Anatolian Fault along the northern margin of the Sea of Marmara, where structural data [*Le Pichon et al.*, 2001] and seismic fault plane solutions (in particular the earthquake of 28 February 2002, discussed by *Le Pichon et al.* [2003]) indicate the presence of an essentially vertical strike-slip fault. [*Meade et al.*, 2002] had noted that four sites to the north of the Sea of Marmara appear to show no elastic effect. To account for this absence of elastic effect, they had to place the fault as far as possible from these sites, along the southern margin of the sea, and use a quite shallow 6.5 km locking depth. Placing the fault where it is actually mapped, (i.e., much closer to the sites, along the northern margin), leads to the conclusion that the fault is unlocked there or that it has a very shallow dip to the south, which is excluded by the structural and seismological data. *Le Pichon et al.* [2003] demonstrated that, assuming asymmetry, the data could be accounted for with a locked fault with an expected 10.5 km locking depth along the northern margin. However, as said, the ratio of asymmetry is very large, about 10 (Figure 2).

Table 1. Model Parameters for Interseismic Loading Analysis[a]

	R	s, mm yr^{-1}	D, km	RMS, mm yr^{-1}
Marmara Sea				
Preferred model	9.7	23.0	10.5	0.42
Sumatra				
Preferred model	27.5	18.9	*9.0*	4.10
Alternative model	15.0	22.3	27.1	3.78
Point Arena				
Preferred model[b]	1.6	16.0	*11.0*	1.29
Alternative model[c]	1.3	13.9	*14.9*	1.34
Symmetric model	*1.0*	15.7	*11.0*	1.46
Point Reyes				
Preferred model[d]	1.1	19.7	*11.0*	1.46

[a]Italic values are fixed in the inversion. R is the contrast in rigidity, defined by the ratio in interseismic fault-parallel motion accommodated on both sides of main strike-slip fault; s is the total slip rate; D is locking depth; and RMS is root mean square.
[b]Locking depth on Ma'acama fault (MF) is set to 12 km, and the slip rate on the MF is solved to be 10.7 mm yr^{-1}. See text for more details.
[c]Locking depth and slip rate along MF are set to be those obtained by *Freymueller et al.* [1999]: 13.4 km and 13.9 mm yr^{-1}, respectively.
[d]Slip rates of Rodgers Creek and Green Valley faults are set to 9.0 and 5.0 mm yr^{-1} [*WGCEP*, 2003].

[12] *Le Pichon et al.* [2003] suggested that this large ratio could be in part due to the thick layer of water and unconsolidated sediments to the south of the fault, following a suggestion of J. Rice [see *Le Pichon et al.*, 2003]. Another contributing factor could be the presence of an asymmetry in the properties of the viscous layer that lies below the brittle layer. The deformation of the free surface produced throughout the earthquake cycle by slippage on a long strike-slip fault in an Earth model consisting of an elastic plate overlying a viscoelastic half-space can be duplicated by prescribed slip on a vertical fault embedded in an elastic half-space [*Savage*, 1990]. Thus the effects of the asymmetry of the viscous layer will appear to be incorporated into the elastic effects. This may account for the presence of ratios of strain that are significantly larger than 2.5. An estimate of this asymmetry due to the superposition of both effects can be simply obtained using the approach of *Savage* [1990] as discussed elsewhere [e.g., *Lisowski et al.*, 1991; *Savage and Lisowski*, 1998]. Also, postseismic motion may contribute to the asymmetry as well [*Kenner and Segall*, 1999, 2003]. However, it is unlikely that significant postseismic effects of the 1999 Kocaeli earthquake, immediately to the east of the Sea of Marmara, extended so far to the west within the sea. Moreover, the geodetic data that were used [*Meade et al.*, 2002] were obtained before the 1999 Kocaeli earthquake. Finally, the estimates of rigidity based on seismic velocities give "dynamic" elastic parameters that might be quite different from static ones. *Ciccotti and Mulargia* [2004] state that we can exclude significant dependence on frequency for the rocks in undamaged conditions. However, they believe that the static response of damaged rocks to large-scale stresses could be quite different from that estimated by seismic measurements. There is little doubt that the rocks below the northern Sea of Marmara are affected by many faults and thus that the static elastic parameters might be quite different from the dynamic ones.

Alternatively, different rheologies may prevail on both sides of the fault.

[13] *Le Pichon et al.* [2003] proposed that the western North Anatolian Fault in the Sea of Marmara follows the northern margin because it juxtaposes two different geologic materials. This asymmetry has since been amplified by a vertical offset of the basement of several kilometers and by the fact that the crust in the trough is highly sheared and faulted.

2.2. Great Sumatra Fault Near Lake Toba

[14] A remarkable example of asymmetry in interseismic strain has been published [*Genrich et al.*, 2000] for the part of the Great Sumatra Fault (GSF) where it follows the western edge of the caldera occupied by lake Toba (Figure 1). This remarkably straight 200 km long segment of fault, called the Renun segment [*Sieh and Natawidjaja*, 2000] is the longest segment of the Sumatra Fault. It traverses the western flank of the 80–100 km Toba caldera [*Bellier and Sébrier*, 1994; *Sieh and Natawidjaja*, 2000] (Figure 1). A great part of this segment traverses a thick 73,000 years old pyroclastic flow deposit [*Sieh and Natawidjaja*, 2000]. When *Genrich et al.* [2000] inverted GPS measurements for the position of the fault assuming symmetry in strain, they obtained offsets of 24 and 14 km to the west with respect to the actual position of the fault at the surface based on two transects situated 40 km apart. They excluded the possibility of a very shallow dip to the southwest of the fault plane, because fault plane solutions of nearby recent earthquakes show no significant deviation from the vertical. They do mention as a possibility heterogeneity in the elastic properties of the upper crust.

[15] To investigate this latter explanation, we reevaluate their GPS observations along the Sidikalang and Dolok Sanggul transects west of lake Toba, north central Sulawesi, where the elastic contrast is expected to be significant (Figure 1). Observed velocities are presented in a Eurasia reference frame defined by *Genrich et al.* [2000]. Although they acknowledged that eastern Sumatra (i.e., the region east of the GSF) is part of the Sunda block, whose independent motion from Eurasia has now become undisputed [e.g., *Simons et al.*, 1999], almost all measurements on the eastern Sumatran margin are insignificantly different from zero. For that reason, and also because we want to be able to compare our results directly with the published results [*Genrich et al.*, 2000] and not introduce any further model uncertainties, we use the same data as have been published (except for the exclusion of stations K319, K381, and K424, which all showed very anomalous motions compared to nearby stations). We also assume two-dimensionality although this strong asymmetry is only present over a total length of probably less than 200 km. However, 70% of the elastic deformation occurs over a distance of twice the locking depth, which is about one tenth of the length of this asymmetric zone. Thus, as a first approximation, our modeling should determine the ratio of asymmetry. When we fix the locking depth to 9 km, in conformity with *Genrich et al.* [2000], we obtain a best fit model (RMS = 4.1 mm yr^{-1}) with a total fault-parallel slip rate of 18.9 mm yr^{-1}, with $R \approx 28$. That is, the northeastern side of the GSF moves only 0.7 mm yr^{-1} because of the elastic loading effect, while on the southwestern side the remaining

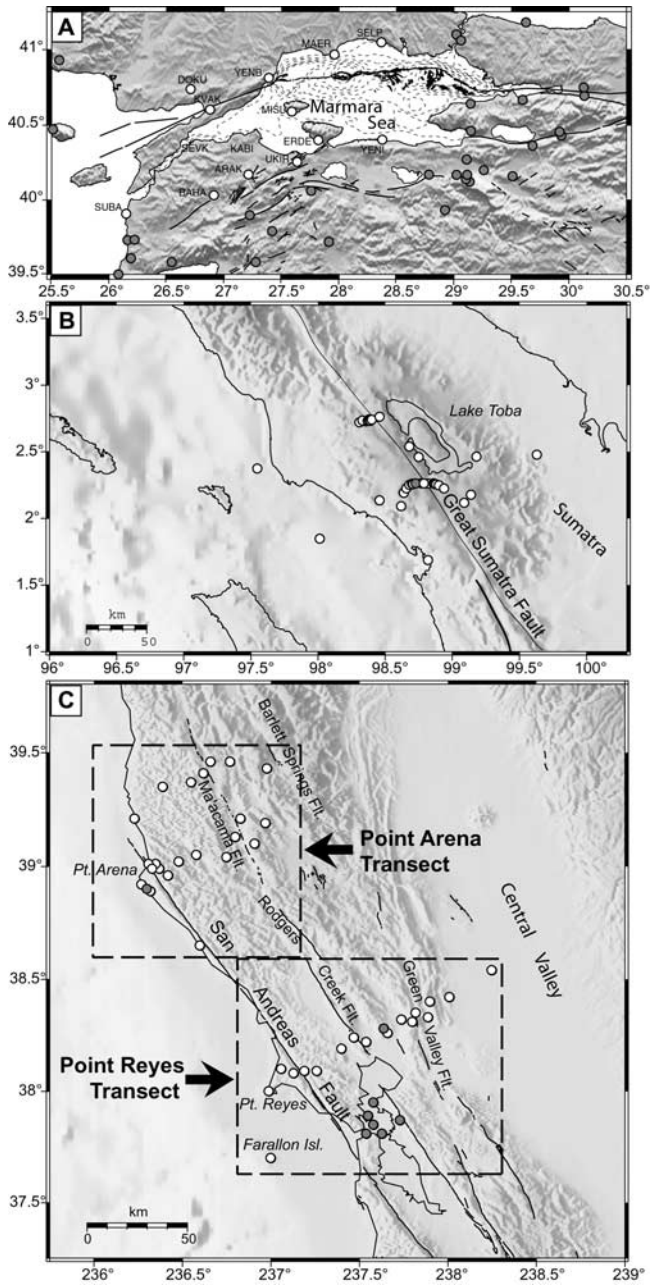

Figure 1. (a) Sea of Marmara region, Turkey. GPS positions from *Meade et al.* [2002] and fault data adapted from *Le Pichon et al.* [2003]. (b) Northwest Sumatra region, Indonesia. GPS positions are from *Genrich et al.* [2000] and fault data from *Sieh and Natawidjaja* [2000]. (c) Point Arena and Point Reyes transects, northern California. GPS positions are from *Freymueller et al.* [1999] and *Savage et al.* [2004] and historic and Holocene faults are from *Jennings* [1992]. White circles indicate site locations of used GPS velocities (grey circles are excluded sites (see text)).

18.2 mm yr^{-1} are distributed over a distance of ~100 km in a direction normal to the fault azimuth (Figure 3). In an alternative model, in which we do not fix the locking depth, we resolve D = 27.1 km, s = 22.3 mm yr^{-1}, and $R \approx 15$

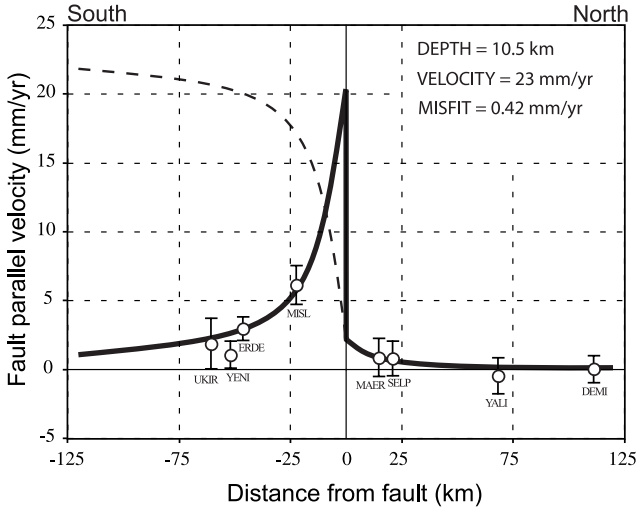

Figure 2. Observed and modeled fault parallel motions subject to a locked fault above a screw dislocation along the North Anatolian Fault in the sea of Marmara after *Le Pichon et al.* [2003]. Observations are from *Meade et al.* [2002]. The total fault velocity is imposed, but the locked depth and the asymmetry ratio are inverted. The solid curve shows the elastic effect versus distance of the fault, that is, $[s(-\infty) - s(x)]$ in $x < 0$ and $[s(x) - s(+\infty)]$ in $x > 0$. The dashed line shows the total velocity curve with respect to the north. (Note that the notations and definitions are different here than in equation (1).)

(RMS = 3.8 mm yr^{-1}). We discard this latter model based on the anomalously large value for the locking depth.

[16] Taken at face value, an R of 28 implies a ratio of about 3 in seismic velocities, if it is entirely explained by an elasticity contrast. This is not impossible if the caldera is underlain by a plug of intrusive massive rock as observed underneath the Etna volcano [*Aloisi et al.*, 2002; *Chiarabba et al.*, 2000; *Hirn et al.*, 1991; *Laigle and Hirn*, 1999; *Laigle et al.*, 2000] adjacent to a thick pile of tuffs and sediment. Underneath Etna, the high-velocity plug may have a P wave velocity ratio as high as 2 with the surrounding material [*Aloisi et al.*, 2002]. Also, the existence of such high-velocity plugs has been demonstrated underneath other volcanoes such as Mt St Helens, Redoubt, and Hawaii (see discussion by *Aloisi et al.* [2002]). We conclude that it is reasonable to expect a large elasticity contrast between the two sides of the fault there and this contrast accounts in large part for the absence of significant elastic interseismic loading on the caldera side of the fault.

2.3. Northern San Andreas Fault

[17] We have mentioned earlier that the northern section of the SAF occupies a zone of transition between thick oceanic lithosphere to the southwest and thin continental lithosphere to the northeast [*Melbourne and Helmberger*, 2001]. We mentioned further that asymmetry in interseismic strain has been described and discussed at the level of the Point Reyes section since *Prescott and Yu* [1986] and at the level of Point Arena section by *Freymueller et al.* [1999]. *Henstock et al.* [1997] studied a seismic profile north of Point Arena, California (see Figure 1), where the crust, including the Moho, is offset several kilometers upward on the ocean side by the SAF that appears to be subvertical. As a result, the rigidity, taking its average value over a width of about 10 km on both sides of the fault, is systematically higher to the southwest of the SAF than to the northeast. Because of this offset, the rigidity ratio is about 1.2–1.3 over the upper section of crust and becomes larger below 10 km (A. Levander, personal communication, 2003). Unfortunately, the SAF is close to the shore. Thus the effect of this asymmetry on the interseismic strain, as measured by geodesy, is difficult to test. Several studies [*Parsons*, 1998; *Parsons and Hart*, 1999; *Parsons et al.*, 2002] have shown that the San Andreas and Hayward faults in the San Fancisco Bay area are subvertical at least within the brittle portion of the crust. *Castillo and Ellsworth* [1993] show that the dips of the faults east of San Andreas are subvertical at the level of Point Arena and to the south of it. Thus we can assume that this strike-slip system of faults is subvertical and any asymmetry we may find is unlikely to be an effect of having a dipping fault.

[18] A geodetic study of the SAF near Point Arena has been published [*Freymueller et al.*, 1999]. This section spans not only the SAF, but also the Ma'acama (MF) and Bartlett Spring (BSF) faults (Figures 1 and 3). Original data were in a Pacific (PA) fixed reference frame, which we have adopted. We combine the Ukias and Willits profiles and take into account the elastic loading expected along the MF. That is, before analyzing the loading along the SAF we 'correct' the interseismic velocities by adding to the observed velocities the predicted elastic displacements given the slip rates and locking depths for the MF [*Freymueller et al.*, 1999]. We do not assume any contrast in rigidity over the MF when we calculate the predicted elastic displacements. Possible elastic loading effects due to a locked BSF are not considered because it is believed to be far enough to have no effect on our analysis and also because most of the motion is probably relieved by creep [*Freymueller et al.*, 1999]. Site HBLF, located just west of the SAF, shows anomalously fast motions, and we have discarded it for this analysis. With a locking depth fixed at 14.9 km, our best fit model (RMS = 1.3 mm yr^{-1}) constrains the total SAF slip rate to 13.9 mm yr^{-1} with $R = 1.3$. Our obtained slip rate is considerably lower than both the 17.4 mm yr^{-1} obtained from the symmetric elastic loading modeling [*Freymueller et al.*, 1999] and the 24 mm yr^{-1} that is the most recent estimated geologic rate [*Working Group on California Earthquake Probabilities* (*WGCEP*), 2003]. It should be noted, however, that SAF fault parameters, including our obtained R value, for the Point Arena section are generally ill-constrained by the geodetic observations, because there is a only a small number of sites on the Pacific side of SAF (particularly after we remove HBLF) and these sites are all located very close to the fault (Figures 1 and 4). In addition, our results are dependent on the assumed slip rate on the MF and locking depths for the SAF and MF taken from *Freymueller et al.* [1999]. Particularly the locking depths are much larger than those inferred geologically or geodetically farther to the south [*Prescott et al.*, 2001; *WGCEP*, 2003]. We thus set up an alternative, and preferred, model in which we fix the locking depths of SAF and MF to 11 and 12 km, respectively [*WGCEP*, 2003], and solve for the slip rate on MF when solving for the asymmetric slip loading on the

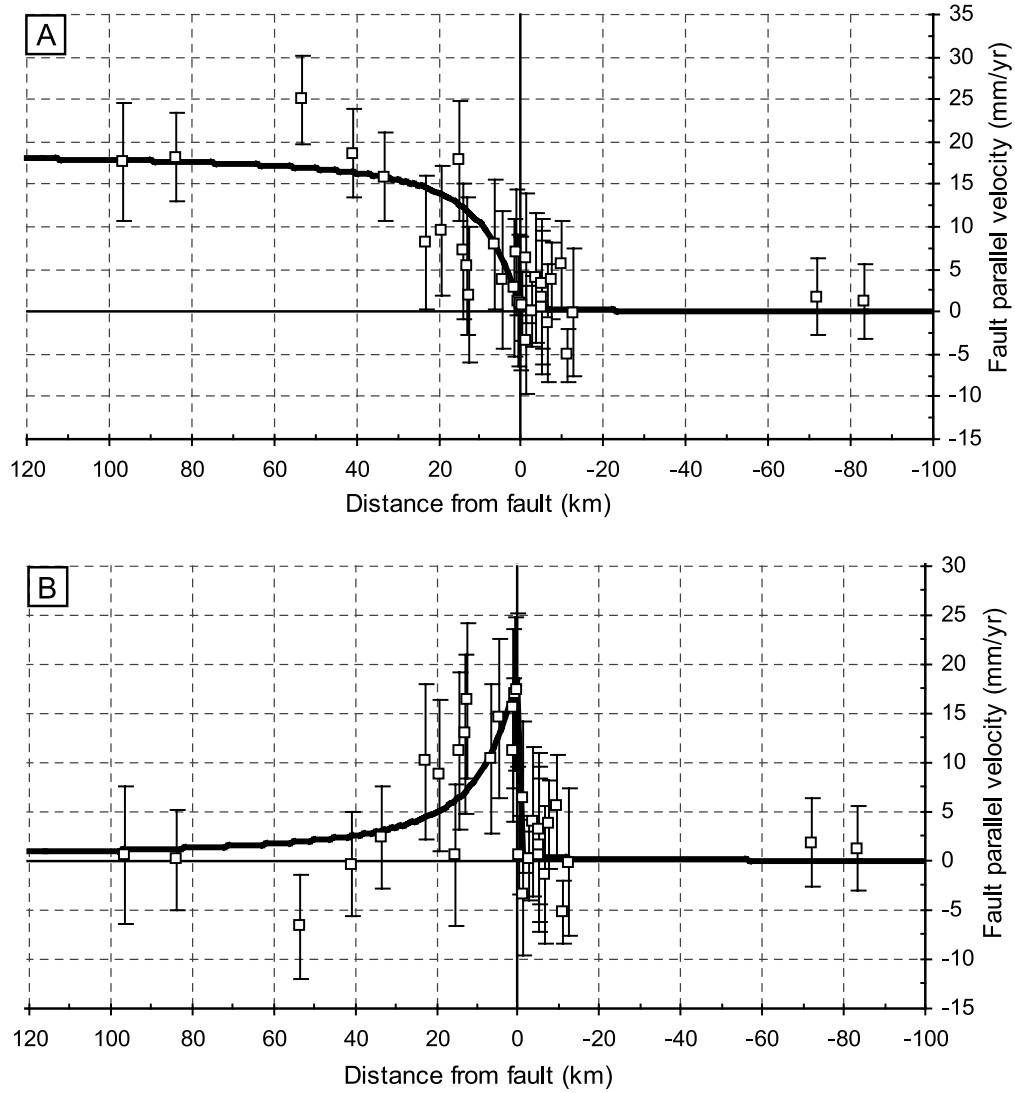

Figure 3. (a) Observed and (preferred) modeled fault parallel motions along the Sumatra Fault near lake Toba caldera. Observations are from *Genrich et al.* [2000] relative to stable Sunda/Eurasia plate for the Sidikalang and Dolok Sanguul transects. (b) Same as in Figure 3a but only showing the effect of elastic loading itself along the main fault. Uncertainties in observed velocities represent one standard uncertainty.

SAF as well. Although the total misfit to the data remains unchanged to 1.3 mm yr^{-1}, we obtain significantly different values for s and R of 16.0 mm yr^{-1} and 1.6, respectively (Figure 4 and Table 1). For this model we find a slip rate on the MF of 10.7 mm yr^{-1}, as opposed to the published 13.9 mm yr^{-1} [*Freymueller et al.*, 1999]. When constraining elastic properties to be equal on both sides of the SAF, the RMS increases to 1.5 mm yr^{-1} while the total slip rate on the SAF remains rather constant at 15.7 mm yr^{-1}.

[19] Farther south, the Point Reyes section of the SAF is the one first discussed for its asymmetry as measured by Geodolite [*Prescott and Yu*, 1986]. Because there is a site on Farallon island, the maximum distance to the fault on the ocean side is nearly 40 km compared to about 7 km for the Point Arena profile (Figure 1). We use the most recent GPS velocities [*Savage et al.*, 2004] along an array that spans from Farallon Island to the Great Valley, crossing SAF, Rodgers Creek (RCF), and Green Valley (GVF) faults. Earlier GPS velocities were presented and interpreted in terms of slip rates and locking depths by *Prescott et al.* [2001]. The data are presented in a North American (NA) reference frame, which we adopt. We exclude station HENN (which is reported to behave anomalously [*Prescott et al.*, 2001]) as well as all stations in the central San Francisco Bay area in order to avoid complexities related to along strike changes in fault positions. As we do for Point Arena, we take into account the elastic loading effects of more inland faults; i.e., RCF and GVF. For all faults we have set the locking depths to the values of *WGCEP* [2003], as was done by *Prescott et al.* [2001]. We have tested models in which we either constrain the slip rates of the RCF and GVF to the values obtained by *Prescott et al.* [2001] (10.3 and 8.2 mm yr^{-1}, respectively) or to the geologic values (9.0 and 5.0 mm yr^{-1}, respectively [*WGCEP*, 2003]) (Table 1)

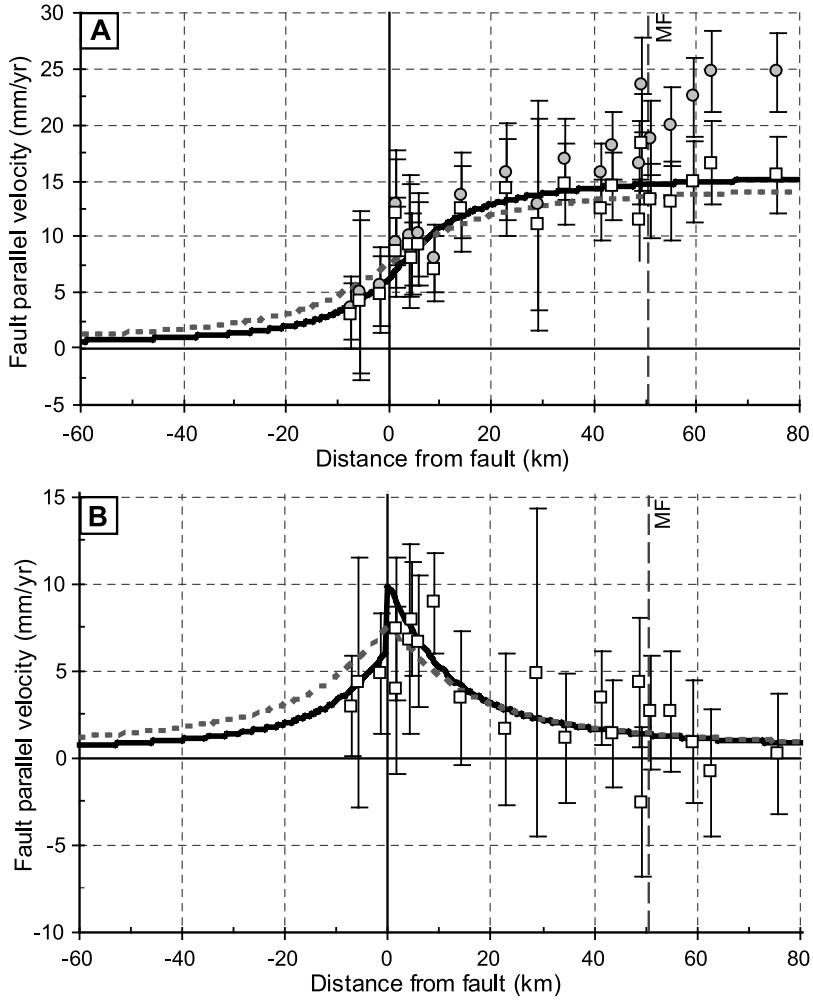

Figure 4. As in Figure 2, but for Ukiah and Willits transects near Point Arena, California. Observations are from *Freymueller et al.* [1999] relative to stable Pacific plate. Solid dots are actual data. Open squares are data corrected for the elastic effect of the Ma'acama fault (MF). Dotted curve in Figure 4b is for a case of symmetric loading on both sides of the fault.

We prefer the latter, partly because there are inconsistencies between the velocities analyzed by *Prescott et al.* [2001] and those used here from *Savage et al.* [2004]. Because for neither side of the SAF do the GPS velocities in this reference frame go to zero, we have to incorporate an additional parameter; the asymptotic total slip rate value west of the fault, analogous to the total PA-NA plate motion. For our preferred model (RMS = 1.5 mm yr^{-1}) we obtain an asymptotic value of 45.6 mm yr^{-1}, with s = 19.7 mm yr^{-1}, and R = 1.1. The elastic loading curve and fit to the data are shown in Figure 5. Our obtained slip rate is a little slower than the previous geodetic estimate of 20.8 mm yr^{-1} [*Prescott et al.*, 2001] and both are much lower than the geologic estimate of 24 mm yr^{-1} [*WGCEP*, 2003]. In light of this, it is important to point out that the GPS velocities [*Prescott et al.*, 2001; *Savage et al.*, 2004] in the westernmost part of the array, and therefore the asymptotic velocity obtained here, are relatively slow compared to expected PA-NA motion of 51.1 mm yr^{-1} [e.g., *DeMets and Dixon*, 1999]. We do not understand this discrepancy, but it could be related to a reference frame problem. In any case, if there is no internal distortion in the network (as is not expected) our analysis should not be significantly affected by the discrepancy in PA-NA motion. We conclude that we do not detect significant asymmetry near Point Reyes. This is surprising as this profile, as mentioned above, is the one where a strong asymmetry had been measured by Geodolite and abundantly discussed in the literature.

3. Coseismic Elastic Rebound During the 1906 San Francisco Earthquake

[20] We wish to quantify the asymmetry in coseismic deformation during the 1906 earthquake using the same two-dimensional screw dislocation model. We are aware that the assumption of two dimensionality is here less justified than for the interseismic motion. The reader is referred to other work [e.g., *Matthews and Segall*, 1993; *Thatcher*, 1975b; *Thatcher et al.*, 1997] for a more complete analysis. However, these papers assume symmetry of deformation. As mentioned earlier, *Kenner and Segall* [2003] recognize significant asymmetry in the postseismic and interseismic deformation in northern California with respect to the trace of the San Andreas fault, but they attribute this

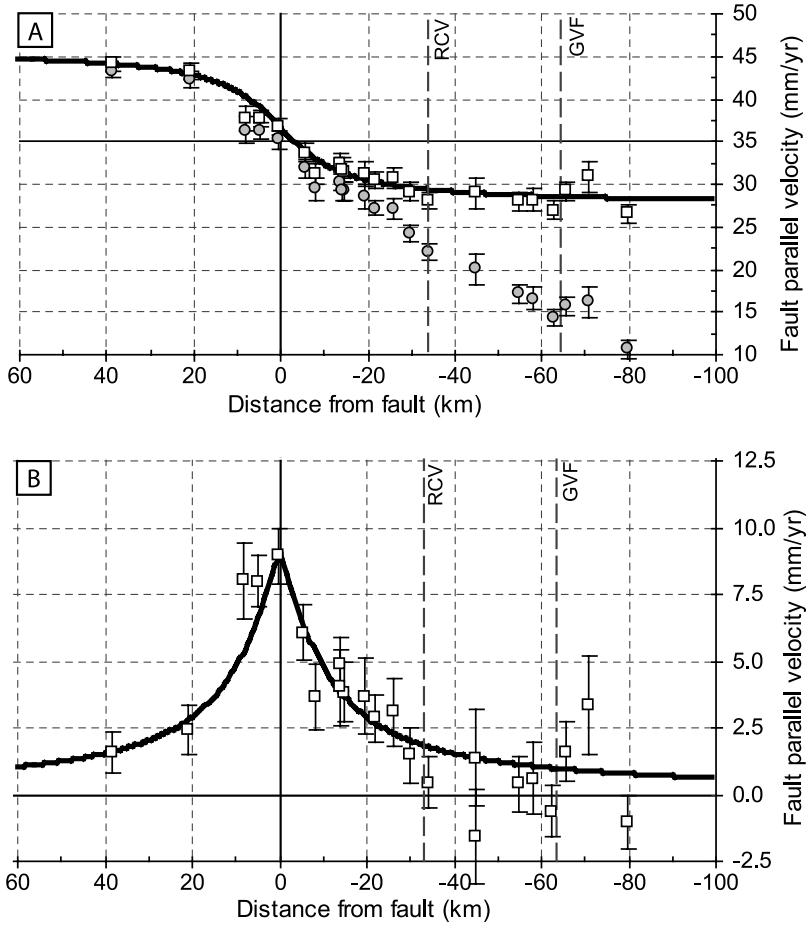

Figure 5. Same as Figures 2 and 3, but for a transect near Point Reyes, California. Observations from *Savage et al.* [2004] relative to stable North America. Open squares are corrected for the effect of loading along the Rogers Creek Fault (RCF) and the Green Valley Fault (GVF).

asymmetry to the presence of discrete shear zones within the lower crust below each of the three subparallel faults. They do not consider the possibility of a bimaterial San Andreas fault. This we do below.

[21] At the Earth's surface, the horizontal displacement field $y(x)$ that reflects the elastic rebound during an earthquake rupture can be expressed by replacing $v(x)$ in (1), by assuming D to be the downdip width of rupture (assuming the earthquake breaks the surface), and by expressing the total slip rate s in terms of total offset d, where $d = d_1 + d_2$;

$$y(x) = 2\frac{d_2}{\pi}\tan^{-1}\left(\frac{x}{D}\right) - d_2; \qquad x > 0$$
$$y(x) = 2\frac{d_1}{\pi}\tan^{-1}\left(\frac{x}{D}\right) + d_1; \qquad x < 0 \tag{2}$$

This case is for a right-lateral rupture, with displacements being relative to the fault (or far-field). Partial offsets d_1 and d_2 are positive, with d_1 and d_2 recovered on the fault's side where $x \to -\infty$ or $x \to \infty$, respectively. As above, the ratio d_2/d_1 will be expressed as R.

[22] We use the observed coseismic displacement of the 1906 San Francisco earthquake [*Hayford and Baldwinn*, 1908] to model possible nonsymmetric relaxation along the Point Arena and Point Reyes section of the SAF. Because observations are sparse (particularly for Point Reyes), we eliminate one free parameter by fixing d to the observed coseismic displacements [*Lawson*, 1908; *Thatcher*, 1975a; *Thatcher et al.*, 1997]. Surface offsets near Point Arena were observed between 3 and 5 m, and along the Point Reyes portion of the SAF they measured between 4 and 6 m. For both fault sections we take the maximum value, because we find that for any smaller value of d the data misfits become very large. (In fact, for a model with d unconstrained, we obtain 5.1 and 6.2 m for the Point Arena and Point Reyes sections, respectively, close to the maximum observed, and close to those estimated using the same geodetic data but with the assumption of lateral symmetry [*Thatcher*, 1975a].) In our best fit models (RMS = 0.09 m and 0.02 m for Point Arena and Point Reyes profiles, respectively), in which we also solve for D, we find that for Point Arena the NE side of the fault has relaxed 1.2 times as much as the Pacific side, and for Point Reyes $R \approx 1.7$ (Figure 6). As reference, and to acknowledge that data points are sparse and uncertainties unknown, we also show predicted coseismic displacements for several other values of R (Figure 6). In our best fit models D is 9.7 and 10.5 km for the Point Arena and Point Reyes sections, respectively. These values are very close to the 10 km obtained using the assumption of lateral symmetry [*Thatcher*, 1975a].

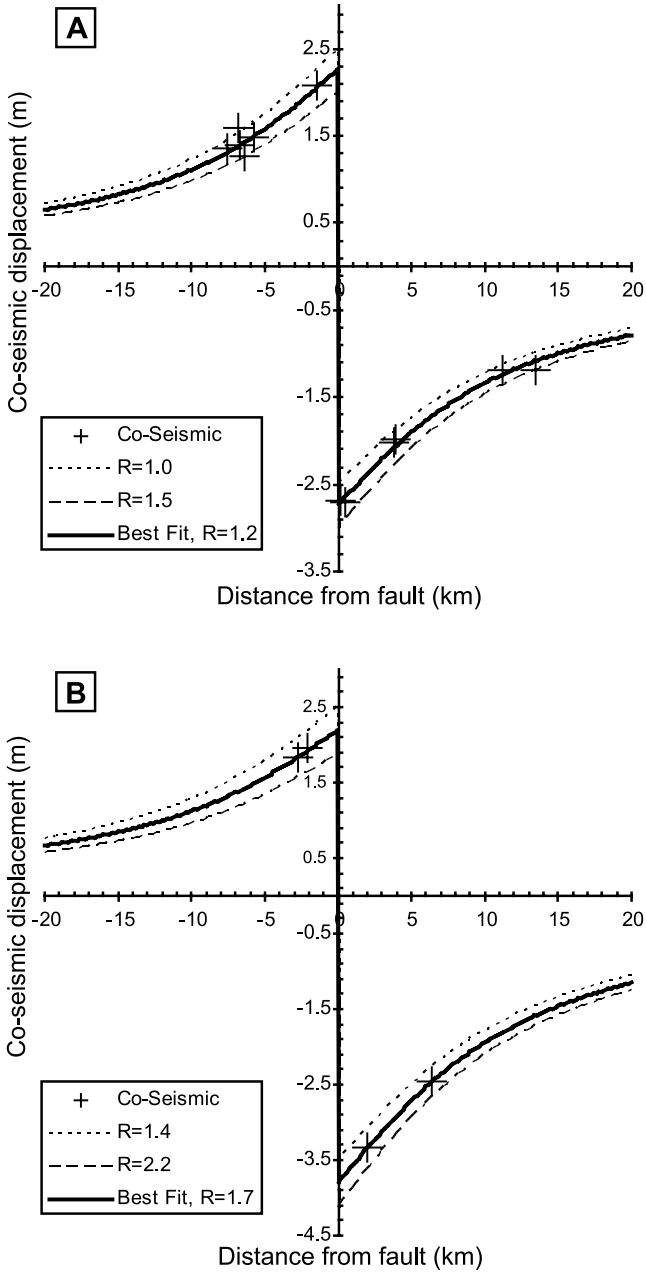

Figure 6. Observed [*Lawson*, 1908; *Thatcher*, 1975a; *Thatcher et al.*, 1997] and modeled coseismic displacements subject to elastic rebound of a fault segment above a screw dislocation during the 1906 San Francisco earthquake data for (a) Point Arena, California, and (b) Point Reyes, California. Best fit model as well as other predicted displacements curves, based on different contrasts in rigidity R, are drawn by dashed curves.

[23] None of the fits of the interseismic and coseismic effects along these two sections of the northern SAF considered alone have a demonstrative value of the presence of significant asymmetry. However, we consider as significant the facts that the more rigid side found for both the interseismic and the coseismic effects is always the southwestern side, as expected from geology and seismology, and that the elasticity ratio values obtained by the interseismic and coseismic modeling are consistent with each other within the relatively large uncertainties of this type of inversion.

4. Discussion and Conclusion

[24] Contrasts in seismic velocity across a fault do not usually exceed 1.35 [*Ben-Zion and Andrews*, 1998]. Because the elastic parameter varies approximately as the seismic velocity to the third power (see above), the maximum elastic parameter ratio expected is about 2.5 ($\sim 1.35^3$). Yet we have documented cases where the apparent ratio is significantly larger. As the typical range of average values of the elastic parameter is an order of magnitude from mantle to sediment, (e.g., from peridotite ($14-16 \times 10^{10}$ Pa) to shale ($1-3 \times 10^{10}$ Pa)), the ratio is unlikely to exceed an order of magnitude anywhere. However, this does not take into account extreme weakening by the presence of gauges, hydraulic quasi-lithostatic pressure, and the effect of high temperature. In addition, other effects such as the difference in altitude on both sides of the fault, for example along a continental margin, may accentuate the average contrast. Another important contributing factor may be the presence of an asymmetry in the viscous layer that lies below the brittle layer. Then postseismic effects should also be asymmetric and may be superposed to interseismic effects [*Kenner and Segall*, 1999, 2003]. Finally, the estimates of rigidity based on seismic velocities give dynamic elastic parameters that might be quite different from static ones. Several of these causes may combine to explain the very high ratios that we documented in this study along the North Anatolian Fault in the Sea of Marmara and along the Sumatra Fault along the Toba caldera.

[25] The existence of large asymmetric elastic loading along the North Anatolian Fault that follows the northern margin of the Sea of Marmara may be especially significant. The fault appeared to have followed a fundamental paleotectonic boundary [*Le Pichon et al.*, 2003; *Sengör*, 1979]. Then as the Marmara depression was formed, during a first pull-apart tectonic phase [*Rangin et al.*, 2004], the fault was trapped within it trying to follow one of its boundaries. In the same way, the western North Anatolian Fault, farther west, in the Aegean Sea, appears to be trapped by the preexisting north Aegean and Saros troughs in which it tends to follow one of the margins [*Papanikolaou et al.*, 2002]. The margins of these troughs are the sites of strong heterogeneity of material. Both in these troughs and within the Sea of Marmara, there is a vertical offset of the basement of several kilometers and the crust in the trough is highly sheared and faulted. These preexisting troughs, because of their built-in asymmetry, act as traps for the fault. The same process may exist along other large faults such as the Dead Sea fault.

[26] Another remarkable example of measured asymmetry in interseismic elastic deformation is along the northern Sumatra fault near lake Toba caldera and appears to be related to the contrast between the massive igneous body below the caldera and the adjacent fractured and less dense material. The case for the northern SAF is different. There, asymmetry in the structure of the lithosphere and asthenosphere and in the properties of the geological formations in the upper crust have long been documented and has been

recognized on the basis of geodetic data. Thus this is one of the places where asymmetry both in interseismic and coseismic effects should be expected. We have tested two portions of the northern SAF where asymmetry had previously been reported by some authors [e.g., *Freymueller et al.*, 1999; *Kenner and Segall*, 2003; *Lisowski et al.*, 1991; *Reid*, 1910]. We have found indeed an asymmetry in the present interseismic effects and in the coseismic motions of the 1906 San Francisco earthquake for the Point Arena and Point Reyes transects. In some cases, however, the found asymmetry is not significant, and may indeed be hard to resolve (see, for example, the interseismic displacements for Point Reyes (Figure 5)). The demonstration that asymmetry exists for any individual profiles is not necessarily a strong argument. However, the fact that all results (interseismic and coseismic) are consistent between the two profiles is encouraging. That is, the southwest side of the fault is systematically more rigid than the northeast one, as expected.

[27] We are puzzled by the fact that asymmetry has not been more widely detected in interferometric studies of large faults. Small asymmetric ratios of 1.2 to 1.4 may be difficult to detect, as it is always possible to account for them through, for example, slight changes in the dip of the fault. This point should be explored by systematic studies both of the fault structure and the different earthquake deformation cycles, keeping open the possibility of elastic and viscous asymmetry across the fault.

[28] **Acknowledgments.** The first author started this work while on a sabbatical at the Department of Earth Sciences at Rice University. Discussions with A. Levander on the crustal structure of northern California were especially helpful. Y. Ben Zion, F. Pollitz, J. Rice, J. C. Savage, P. Segall, and W. Thatcher introduced us to this difficult subject, although they are in no way responsible for what is written in this paper. We thank M. Bonafede and E. Rivalta and the associate editor for their careful reviews. This work was financed by Collège de France.

References

Aloisi, M., O. Cocina, G. Neri, B. Orecchio, and E. Privitera (2002), Seismic tomography of the crust underneath the Etna volcano, Sicily, *Phys. Earth Planet. Inter.*, *134*, 139–155.

Andrews, D. J., and Y. Ben-Zion (1997), Wrinkle-like pulse on a fault between different materials, *J. Geophys. Res.*, *102*, 553–5571.

Bellier, O., and M. Sébrier (1994), Relationship between tectonism and volcanism along the Great Sumatran Fault Zone deduced by SPOT image analyses, *Tectonophysics*, *233*, 215–231.

Ben-Zion, Y., and D. J. Andrews (1998), Properties and implications of dynamic rupture along a material interface, *Bull. Seismol. Soc. Am.*, *88*, 1085–1094.

Ben-Zion, Y., and C. G. Sammis (2003), Characterization of fault zones, *Pure Appl. Geophys.*, *160*, 677–715.

Castillo, D., and W. L. Ellsworth (1993), Seismotectonics of the San Andreas Fault System between Point Arena and Cape Mendocino in northern California: Implications for the development and evolution of a young transform, *J. Geophys. Res.*, *98*, 6543–6560.

Chen, Q., and J. T. Freymueller (2002), Geodetic evidence for a Near-Fault Compliant zone along the San Andreas Fault in the San Francisco Bay area, *Bull. Seismol. Soc. Am.*, *92*, 656–671.

Chiarabba, C., A. Amato, E. Boschi, and F. Barberi (2000), Recent seismicity and tomographic modeling of the Mount Etna plumbing system, *J. Geophys. Res.*, *105*, 10,923–10,928.

Chinnery, M. A. (1961), The deformation of the ground around surface faults, *Bull. Seismol. Soc. Am.*, *51*, 355–372.

Christensen, N. I., and W. D. Mooney (1995), Seismic velocity structure and composition of the continental crust: a global view, *J. Geophys. Res.*, *100*, 9761–9788.

Ciccotti, M., and F. Mulargia (2004), Differences between static and dynamic elastic moduli of a typical seismogenic rock, *Geophys. J. Int.*, *157*(1), 474–477.

DeMets, C., and T. H. Dixon (1999), New kinematic models for Pacific-North America motion from 3 Ma to present, I: Evidence for steady motion and biases in the NUVEL-1A model, *Geophys. Res. Lett.*, *26*, 1921–1924.

Freymueller, J. T., M. H. Murray, P. Segall, and D. Castillo (1999), Kinematics of the Pacific-North America plate boundary zone, northern California, *J. Geophys. Res.*, *104*, 7419–7441.

Genrich, J. F., Y. Bock, R. McCaffrey, L. Prawirodirjo, C. W. Stevens, S. S. O. Puntodewo, C. Subarya, and S. Wdowinski (2000), Distribution of slip at the northern Sumatran fault system, *J. Geophys. Res.*, *105*, 28,327–28,341.

Hayford, J. F., and A. L. Baldwinn (1908), The earth movements in the California earthquake of 1906, in *The California Earthquake of April 18, 1906, Report of the State Earthquake Investigation Commission*, pp. 114–145, Carnegie Inst. of Washington, Washington, D. C.

Henstock, T. J., A. Levander, and J. A. Hole (1997), Deformation in the lower crust of the San Andreas fault system in northern California, *Science*, *278*, 650–653.

Hirn, A., A. Nercessian, M. Sapin, F. Ferucci, and G. Wittlinger (1991), Seismic heterogeneity of Mount Etna: stucture and activity, *Geophys. J. Int.*, *105*, 139–153.

Jennings, C. W. (1992), Preliminary fault activity map of California, *Calif. Div. Mines Geol. Open File Rep.*, *92-03*.

Kenner, S., and P. Segall (1999), Time-dependence of the stress shadowing effect and its relation to the structure of the lower crust, *Geology*, *27*, 119–122.

Kenner, S. J., and P. Segall (2003), Lower crustal structure in northern California: Implications from strain rate variations following the 1906 San Francisco earthquake, *J. Geophys. Res.*, *108*(B1), 2011, doi:10.1029/2001JB000189.

Laigle, M., and A. Hirn (1999), Explosion-seismic tomography of a magmatic body beneath Etna: volatile discharge and tectonic control of volcanism, *Geophys. Res. Lett.*, *26*, 2665–2668.

Laigle, M., A. Hirn, M. Sapin, J. C. Lépine, J. Diaz, J. Gallart, and R. Nicolich (2000), Mount Etna dense array local earthquake P and S tomography and implications for volcanic plumbing, *J. Geophys. Res.*, *105*, 21,633–21,646.

Lawson, A. C. E. (1908), *The California Earthquake of April 18, 1906: Report of the State Earthquake Investigation Commission*, Carnegie Inst. of Washington, Washington, D. C.

Le Pichon, X., et al. (2001), The active main Marmara fault, *Earth Planet. Sci. Lett.*, *192*, 595–616.

Le Pichon, X., N. Chamot-Rooke, C. Rangin, and A. M. C. Sengör (2003), The North Anatolian fault in the Sea of Marmara, *J. Geophys. Res.*, *108*(B4), 2179, doi:10.1029/2002JB001862.

Li, V. C., and J. R. Rice (1987), Crustal deformation in great California earthquake cycles, *J. Geophys. Res.*, *92*, 11,533–11,551.

Lisowski, M., J. C. Savage, and W. H. Prescott (1991), The velocity field along the San Andreas Fault in central and southern California, *J. Geophys. Res.*, *96*, 8369–8389.

Malservisi, R., K. P. Furlong, and T. H. Dixon (2001), Influence of the earthquake cycle and lithospheric rheology on the dynamics of the eastern California shear zone, *Geophys. Res. Lett.*, *28*, 2731–2734.

Matthews, M. V., and P. Segall (1993), Estimation of depth-dependent fault slip from measured surface deformation with application to the 1906 San Francisco earthquake, *J. Geophys. Res.*, *98*, 12,153–12,163.

Meade, B. J., B. H. Hager, S. C. McClusky, R. Reilinger, S. Ergintav, O. Lenk, A. Barka, and H. Ozener (2002), Estimates of seismic potential in the Marmara Sea region from block models of secular deformation constrained by Global Positioning System measurements, *Bull. Seismol. Soc. Am.*, *92*, 208–215.

Melbourne, T., and D. Helmberger (2001), Mantle control of plate boundary deformation, *Geophys. Res. Lett.*, *28*, 4003–4006.

Papanikolaou, D., M. Alexandri, P. Nomikou, and D. Ballas (2002), Morphotectonic structure of the western part of the North Aegean Basin based on swath bathymetry, *Mar. Geol.*, *190*, 465–492.

Parsons, T. (1998), Seismic reflection evidence that the Hayward fault extends into the lower crust of the San Francisco Bay area, California, *Bull. Seismol. Soc. Am.*, *88*, 1212–1223.

Parsons, T., and P. E. Hart (1999), Dipping San Andreas and Hayward faults revealed beneath San Francisco Bay, California, *Geology*, *27*, 839–842.

Parsons, T., J. McCarthy, P. E. Hart, J. A. Hole, J. Childs, D. H. Oppenheimer, and M. L. Zoback (2002), A review of faults and crustal structure in the San Francisco Bay Area as revealed by seismic studies: 1991–97, in *Crustal Structure of the Coastal and Marine San Francisco Bay Region, California*, edited by T. Parsons, *U.S. Geol. Surv. Prof. Pap.*, *1658*, 119–145.

Peltzer, G., F. Crampé, and G. King (1999), Evidence of nonlinear elasticity of the crust from the Mw7.6 Manyi (Tibet) earthquake, *Science*, *286*, 272–276.

Prescott, W. H., and S. B. Yu (1986), Geodetic measurements of horizontal deformation in the northern San Francisco Bay region, California, *J. Geophys. Res.*, *91*, 7475–7484.

Prescott, W. H., J. C. Savage, J. L. Svarc, and D. Manaker (2001), Deformation across the Pacific-North America plate boundary near San Francisco, California, *J. Geophys. Res.*, *106*, 6673–6682.

Rangin, C., X. Le Pichon, E. Demirbag, and C. Imren (2004), Strain localization in the Sea of Marmara: Propagation of the North Anatolian Fault in a now inactive pull-apart, *Tectonics*, *23*, TC2014, doi:10.1029/2002TC001437.

Reid, H. F. (1910), The mechanics of the earthquake, in *The California Earthquake of April 18, 1906, Report of the State Earthquake Investigation Commission*, vol. II, pp. 15–32, Carnegie Inst. of Washington, Washington, D.C.

Rybicki, K., and K. Kasahara (1977), A strike-slip fault in a laterally inhomogeneous medium, *Tectonophysics*, *42*, 127–138.

Savage, J. C. (1990), Equivalent strike-slip earthquake cycles in half-space and lithosphere-asthenosphere earth models, *J. Geophys. Res.*, *95*, 4873–4879.

Savage, J. C., and R. O. Burford (1973), Geodetic determination of relative plate motion in central California, *J. Geophys. Res.*, *78*, 832–845.

Savage, J. C., and M. Lisowski (1998), Viscoelastic coupling model of the San Andreas Fault along the Big Bend, southern California, *J. Geophys. Res.*, *103*, 7281–7292.

Savage, J. C., W. Gan, W. H. Prescott, and J. L. Svarc (2004), Strain accumulation across the Coast Ranges at the latitude of San Francisco, 1994–2000, *J. Geophys. Res.*, *109*, B03413, doi:10.1029/2003JB002612.

Sengör, A. M. C. (1979), The North Anatolian transform fault: its age, offset and tectonic significance, *J. Geol. Soc. London*, *136*, 269–282.

Sieh, K., and D. Natawidjaja (2000), Neotectonics of the Sumatran fault, Indonesia, *J. Geophys. Res.*, *105*, 28,295–28,326.

Simons, W. J. F., B. A. C. Ambrosius, R. Noomen, D. Angermann, P. Wilson, M. Becker, E. Reinhart, A. Walpersdorf, and C. Vigny (1999), Observing plate motions in SE Asia: Geodetic results of the GEODYSSEA project, *Geophys. Res. Lett.*, *26*, 2081–2084.

Thatcher, W. (1975a), Strain accumulation and release mechanism of the 1906 San Francisco earthquake, *J. Geophys. Res.*, *80*, 4862–4872.

Thatcher, W. (1975b), Strain accumulation on the northern San Andreas fault zone since 1906, *J. Geophys. Res.*, *80*, 4873–4880.

Thatcher, W., G. Marshall, and M. Lisowski (1997), Resolution of fault slip along the 470-km-long rupture of the great 1906 San Francisco earthquake and its implications, *J. Geophys. Res.*, *102*, 5353–5367.

Weertman, J. (1980), Unstable slippage across a fault that separates elastic media of different elastic constants, *J. Geophys. Res.*, *85*, 1455–1461.

Weertman, J., and J. R. Weertman (1964), *Elementary Dislocation Theory*, 213 pp., Macmillan, New York.

Working Group on California Earthquake Probabilities (WGCEP) (2003), Earthquake probabilities in the San Francisco Bay region: 2002–2031, *U.S. Geol. Surv. Open File Rep., 03-214*.

N. Chamot-Rooke, Laboratoire de Géologie, Ecole Normale Supérieure, 24 Rue Lhomond, F-75231 Paris, France.

C. Kreemer, Nevada Bureau of Mines and Geology, University of Nevada, 1664 N Virginia St MS 178, Reno, NV 89557-0000, USA.

X. Le Pichon, Collège de France, Europôle de l'Arbois, F-13545 Aix-en-Provence Cedex 04, France. (lepichon@cdf.u-3mrs.fr)